Atmospheric
Chemistry
and Physics
Discussions

Open Access

EGU

1 **Secondary Organic Aerosols from OH Oxidation of Cyclic Volatile Methyl Siloxanes as an Important**

2 **Si Source in the Atmosphere**

3 Chong Han[1,2], Hongxing Yang[2], Kun Li[1,3], Patrick Lee[1], John Liggio[1], Amy Leithead[1], Shao-Meng Li[4*]

4 [1]Air Quality Research Division, Environment and Climate Change Canada, Toronto, Ontario M3H 5T4,

5 Canada

6 [2]School of Metallurgy, Northeastern University, Shenyang, 110819, China

7 [3]Laboratory of Atmospheric Chemistry, Paul Scherrer Institute, Villigen 5232, Switzerland

8 [4]State Key Joint Laboratory of Environmental Simulation and Pollution Control, College of Environmental

9 Sciences and Engineering, Peking University, Beijing, China 100871

10 **Correspondence**: Shao-Meng Li (shaomeng.li@pku.edu.cn)

11

12 **Short summary:** We presented yields and compositions of Si-containing SOA generated from the reaction

13 of cVMS (D3-D6) with OH radicals. NO_x played negative roles on cVMS SOA formation, while ammonium

14 sulfate seeds enhanced D3-D5 SOA yields at short photochemical ages under high-NO_x conditions. The

15 aerosol mass spectra confirmed that the components of cVMS SOA significantly relied on OH exposure. A

16 global cVMS-derived SOA source strength was estimated to understand SOA formation potentials of cVMS.

17

18 **Abstract**

19   Cyclic volatile methyl siloxanes (cVMS) are active ingredients in widely used consumer products, which

20 can volatilize into the atmosphere, thus attracting much attention due to their potential environmental risks.

21 While in the atmosphere the cVMS undergo oxidation yielding both gaseous and particulate products. The

22 aerosol yields and compositions from the OH oxidation of four cVMS (D3-D6) were determined under low

23   and high-NO$_x$ conditions in an oxidation flow reactor. The aerosol yields progressively increased from D3

24   to D6, consistent with the volatilities and molecule weights of these cVMS. NO$_x$ can restrict the formation

25   of SOA, leading to lower SOA yields under high-NO$_x$ conditions than under low-NO$_x$ conditions, with a

26   yield decrease between 0.05-0.30 depending on the cVMS. Ammonium sulfate seeds exhibited minor

27   impacts on SOA yields under low-NO$_x$ conditions, but significantly increased the SOA yields in the oxidation

28   of D3-D5 at short photochemical ages under high-NO$_x$ conditions. The mass spectra of the SOA showed a

29   dependence of its chemical compositions on OH exposure. At high exposures, equivalent to photochemical

30   ages of >6 days in the atmosphere, D4-D6 SOA mainly consisted of C$_x$H$_y$ and C$_x$H$_y$O$_z$Si$_n$ under low-NO$_x$

31   conditions, whereas they primarily contained N$_m$O$_z$, C$_x$H$_y$, C$_x$H$_y$O$_1$, C$_x$H$_y$O$_{>1}$ and C$_x$H$_y$O$_z$Si$_n$ under high-NO$_x$

32   conditions. Using the yield data from the present study and reported cVMS annual production, a global

33   cVMS-derived SOA source strength is estimated to be 0.16 Tg yr^{-1}, distributed over major urban centers.

34

35   **1 Introduction**

36   Secondary organic aerosols (SOA), which contribute 50-85% to the mass of atmospheric organic aerosols

37   (OA) (Glasius and Goldstein, 2016), are mainly formed via the partitioning of low volatility products from

38   oxidation of volatile organic compounds (VOCs), semi- and intermediate volatile organic

39   compounds(S/IVOCs) (Riipinen et al., 2012). SOA has attracted significant attention due to their important

40   impacts on climate, ecosystems and human health (Berndt et al., 2016). Global budgets of SOA remain an

41   unresolved issue despite extensive research, largely due to uncertainties associated with aerosol yields and

42   the presence of unconsidered SOA precursors.

43   As one type of anthropogenic VOC and potential SOA precursors, cyclic volatile methyl siloxanes (cVMS)

44   are widely used in industrial applications and personal care products (Genualdi et al., 2011; Krogseth et al.,

45   2013a). cVMS have been classified as high-volume chemicals with an annual production of millions of tons

46   globally (Rücker and Kümmerer, 2015; Ahrens et al., 2014). Studies of cVMS in the environment have

47   focused on investigating health and environmental impacts particularly due to their potential persistence,

48   bioaccumulation and toxicity (Guo et al., 2019; Liu et al., 2018; Farasani and Darbre, 2017; Xu et al., 2019;

49   Kim et al., 2018; Coggon et al., 2018). As a result, the European Council has proposed a restriction on the

50   octamethylcyclotetrasiloxane (D4) and decamethylcyclopentasiloxane (D5) content in wash-off personal

51   care products to a limit of 0.1 mass% by 2020. The legislative actions notwithstanding, knowledge of

52   environmental behavior of cVMS remains surprisingly scarce as compared to their applications and

53   economic significance (Rücker and Kümmerer, 2015).

54   It has been estimated that approximately 90% of cVMS are emitted into the atmosphere due to their high

55   saturation vapor pressures (Allen et al., 1997). Gas-phase cVMS have been observed in both indoor and

56   outdoor air. Tang et al. (2015) reported that cVMS accounted for about one third of total VOC mass

57   concentration in a classroom. Outdoor air concentrations of cVMS have also been measured at different sites

58   worldwide (Li et al., 2020; Wang et al., 2018; Rauert et al., 2018), increasing from rural to urban sites and

59   consistent with increasing population density (Rücker and Kümmerer, 2015). For example, at a rural site in

60   Sweden, the concentration of hexamethylcyclotrisiloxane (D3), D4, D5 and dodecamethylcyclohexasiloxane

61   (D6) were 0.94, 3.5, 13 and 1 ng/m^3, respectively (Kierkegaard and Mclachlan, 2013), while they were 18,

62   55, 172 and 14 ng/m^3 in urban areas of Toronto in Canada, respectively (Genualdi et al., 2011; Rauert et al.,

63   2018). cVMS have also been detected in the remote Arctic atmosphere, confirming their long-range transport

64   (Genualdi et al., 2011; Krogseth et al., 2013b). Atmospheric half-lives of cVMS are on the order of 30, 15,

65   10 and 1.6 days for D3-D6, respectively, which allow cVMS to exhibit a hemispherical distribution in the

66   atmosphere (Whelan et al., 2004; Allen et al., 1997; Yucuis et al., 2013; Xiao et al., 2015; Macleod et al.,

Atmospheric
Chemistry
and Physics
Discussions

Open Access

EGU

67   2013). These lifetimes are driven mostly by reactions with the OH radicals (Xiao et al., 2015; Wang et al.,

68   2013), which generate silanols and dimeric products that can be partitioned to condensed phases (Coggon et

69   al., 2018; Sommerlade, 1993; Wu and Johnston, 2016). The loss of cVMS in the atmosphere is slight through

70   O_3 and NO_3 due to their small reaction rates, and by Cl atoms on account of its low concentration (Atkinson,

71   1991; Alton and Browne, 2020).

72   It has been demonstrated that elemental Si is a frequent constituent of nanoparticles in rural and urban

73   areas (Phares et al., 2003; Rhoads, 2003; Bein, 2005; Bzdek et al., 2014) and in remote regions (Li and

74   Winchester, 1990; Li and Winchester, 1993). These Si-containing nanoparticles have previously been

75   attributed to ore smelting processes, but recent studies have shown that Si-containing species are one of the

76   main components in cVMS SOA, suggesting that the oxidation of cVMS may be an important source of Si

77   in atmospheric aerosols (Wu and Johnston, 2016, 2017). In a modeling study, the oxidation products of

78   cVMS (D4, D5 and D6) were considered to quantify the maximum potential for aerosol formation through

79   reactions with the OH radicals (Janechek et al., 2017). Chandramouli and Kamens (2001) demonstrated the

80   gas-particle partitioning of silanols from D5 oxidation by the OH radicals. Wu and Johnston (2016, 2017)

81   analyzed the chemical composition of secondary aerosols from OH oxidation of D4 and D5, showing a large

82   number of monomeric and dimeric products. Janechek et al. (2017, 2019) reported physical properties of

83   SOA generated by OH oxidation of D5, including hygroscopicity, cloud seeding potential and volatility.

84   Charan et al. (2021) measured SOA yields of D5 using chambers and flow tube reactors, indicating necessary

85   conditions when extrapolating SOA yields to the ambient atmosphere. These studies mainly focused on D5

86   and occasionally D4 but rarely others. To better understand the SOA-forming potentials of typical cVMS in

87   the atmosphere, accurate yields and molecular compositions of SOA from the oxidation of cVMS under

88   various atmospheric conditions are needed.

89   In this work, the formation of SOA from the oxidation of four cVMS (D3-D6) by OH radical was

90   investigated in an oxidation flow reactor (OFR). Under various combinations of NO_x and ammonium sulfate

91   seed concentrations, the yields and compositions of SOA formed from the oxidation were measured using a

92   suite of instruments including a scanning mobility particle sizer (SMPS), a proton transfer reaction time of

93   flight mass spectrometer (PTR-ToF-MS) and an aerosol mass spectrometer (AMS). Based on these SOA

94   yields, the contribution of cVMS to SOA in the global atmosphere was estimated using reported cVMS

95   concentrations. The results obtained here can largely improve our understanding of the contribution and

96   composition of SOA from cVMS.

97   **2 Experiments and methods**

98   **2.1 Photo-oxidation experiments**

99   The reactions of cVMS with OH radicals were controlled at a constant temperature (21±1˚C) and relative

100   humidity (35%±2%) in a custom-made oxidation flow reactor (the Environment and Climate Change Canada

101   oxidation flow reactor, ECCC-OFR), which is shown in Fig. S1 of the Supplement and has been described

102   in detail previously (Li et al., 2019a). Briefly, the ECCC-OFR is a fused quartz cylinder (length: 50.8 cm,

103   inner diameter: 20.3 cm) equipped with a conical inlet and 7 outlets. Wall losses of particles and gases in the

104   ECCC-OFR have been shown to be lower than in other OFRs (Huang et al., 2017; Lambe et al., 2011;

105   Simonen et al., 2017; Li et al., 2019a). The length and full angle of cone inlet are 35.6 cm and 30°,

106   respectively, designed to minimize the formation of jetting and recirculation in the OFR. The outlet at the

107   reactor center is a stainless-steel sampling port (inner diameter: 0.18 in) extending 12.7 cm long into the

108   ECCC-OFR. This sampling inlet reduces the impact of potential turbulent eddies caused by the back end of

109   the reactor. The remaining 6 outlets around the perimeter are designed to allow side flows to pass through

110   the OFR as a sheath flow, indirectly reducing wall losses of gases and particles inside the OFR upon sampling.

111   Ozone-free mercury UV lamps for generating OH radicals are housed in small quartz tubes around and in

112   parallel to the quartz reaction cylinder, and a large flow of air through each of these smaller quartz tubes is

113   used to remove the heat produced by the lamps. The relative humidity was adjusted by controlling the ratio

114   of dry air to wet air into the reactor, and was measured using a humidity sensor (Vaisala) at one of the sheath

115   flow outlets (side flows) of the reactor. The volume of the entire ECCC-OFR is about 16 L and the total flow

116   rate is 8 L min^{-1}, leading to a residence time of 2 min in the OFR.

117   OH radicals were produced through the reaction of water vapor with O(^{1}D) formed from O$_3$ photolysis at

118   254 nm. The OH concentration in the ECCC-OFR was regulated by controlling the input voltage and the

119   number of UV lamps. Methanol vapor, introduced into the ECCC-OFR through a bubbler containing

120   methanol solution, was used to determine the OH exposure (i.e., photochemical age) by tracking its decay

121   in the reactor from the reaction with the OH. The decay, or fractional loss, of gas-phase methanol,

122    $[MeOH]/[MeOH]_0$ was measured with the PTR-ToF-MS, and was used to calculate the OH concentration

123   via Equation 1,

124 $$[OH] = -\frac{1}{k_{MeOH}} \ln \frac{[MeOH]}{[MeOH]_0} \tag{1}$$

125   where k_{MeOH} is the second-order rate constant of methanol reaction with OH at 298 K (9.4×10^{-13} cm^3

126   molecule^{-1} s^{-1}). It was noted that the OH exposure measurement was offline, because methanol can affect the

127   OH reactivity with cVMS. Under low and high-NO$_x$ conditions described below, the OH exposure varied in

128   the range of 5.5×10^{10}-1.8×10^{12} and 8.2×10^{10}-1.1×10^{12} molecules cm^{-3} s, respectively. They correspond

129   to 0.4-14.2 and 0.6-8.5 equivalent days (photochemical age), respectively, assuming that an average OH

130   concentration in air is 1.5×10^6 molecules cm^{-3} (Mao et al., 2009).

131   Pure D3-D6 cVMS compounds (solid D3 and liquid D4, D5 and D6) were placed in a glass U-type tube

132   and maintained at the room temperature. Vapors from these compounds (Table S1 of the Supplement) were

Atmospheric
Chemistry
and Physics
Discussions
Open Access
EGU

133   separately introduced into the ECCC-OFR by a small flow of zero air (1-18 mL min^{-1}) passing over the

134   headspace of the U-tube containing the pure compounds. The concentrations of D3-D6 in the ECCC-OFR

135   ranged from 20 to 40 ppb, depending on their volatilities. To study the influence of existing particles on the

136   SOA formation, ammonium sulfate (AS) seed particles were produced using an atomizer, dried by a diffusion

137   dryer and neutralized by a neutralizer and injected into the reactor without size selection. The mass

138   concentration of AS seed particles was approximately 30 μg m^{-3} for all experiments.

139   N$_2$O was used as a source of NO to achieve high-NO$_x$ conditions (Lambe et al., 2017). NO$_x$ conditions

140   were defined by the fate of peroxy radicals (RO$_2$), which was described by the reaction rate ratio (R_{NO}) of

141   RO$_2$ + NO and RO$_2$ + HO$_2$ (Peng et al., 2017). The R_{NO} ratio increases with increasing OH exposures at a

142   constant concentration of N$_2$O (Li et al., 2019b). To achieve a constant branching ratio during the high-NO$_x$

143   experiments, the initial N$_2$O concentration in the OFR was varied (1.6%-8.0%) to maintain an R_{NO} value of

144   20 (Li et al., 2019b), as calculated using a model (OFR Exposures Estimator v3.1) (Peng et al., 2017). A

145   ratio of R_{NO}=20 indicates that 95% of RO$_2$ reacts with NO, ensuring the dominance of RO$_2$ + NO, which

146   represents conditions that are relevant for urban atmosphere (Peng et al., 2019). Under low-NO$_x$ conditions,

147   N$_2$O was not introduced into the OFR, where the RO$_2$ radicals dominantly interacted with HO$_2$ radicals,

148   representing atmospheric scenarios with few NO$_x$ sources.

149   **2.2 Characterization and analysis**

150   The concentrations of cVMS in the OFR were measured online with a proton transfer reaction time of

151   flight mass spectrometer (PTR-ToF-MS, Ionicon Analytik GmbH) (Liggio et al., 2016). The number and

152   mass size distribution of aerosols was monitored using a scanning mobility particle sizer (SMPS, TSI). The

153   mass spectra and elemental composition of aerosols was determined with a high-resolution time-of-flight

154   aerosol mass spectrometer (HR-ToF-AMS, Aerodyne) and analyzed with the AMS analysis software Squirrel

155   (version 1.62G) and Pika (version 1.22G).

156   SOA mass yields (Y) were calculated via Equation 2,

157    $$Y = \frac{\Delta C_{\text{SOA}}}{\Delta C_{\text{cVMS}}}$$ (2)

158   where ΔC_{SOA} and ΔC_{cVMS} are the mass concentrations of SOA formed and cVMS lost, respectively. The mass

159   concentration of SOA was determined by multiplying the effective aerosol density by the integrated SOA

160   volume concentration from the SMPS, subtracting the AS seed volume for experiments with AS seeds. The

161   effective aerosol density (ρ) was calculated for unseeded experiments through the following Equation 3

162   (Lambe et al., 2015),

163    $$\rho = \frac{D_{va}}{D_m}$$ (3)

164   where D_{va} is the vacuum aerodynamic diameter obtained from the HR-ToF-AMS, and D_m is the electric

165   mobility diameter measured by the SMPS. The ρ varied in the range of 1.6-1.8 depending on the cVMS. The

166   same ρ value was also used in the seeded experiments.

167   **3 Results and discussion**

168   **3.1 SOA yields**

169   Figure 1 shows the SOA yields from the photooxidation of the D3-D6 cVMS under low and high-NO$_x$

170   conditions as a function of photochemical age (PA), i.e., time-integrated OH exposure, with and without AS

171   seed particles. SOA yields have been widely used to estimate the potential of precursors to produce aerosol

172   mass (Mcfiggans et al., 2019; Li et al., 2019a; Bruns et al., 2015; Lambe et al., 2015). As shown in Fig. 1,

173   the cVMS SOA yields exhibited an overall increasing trend with PA, expressed in equivalent photochemical

174   days, which agreed with the trend of D5 SOA yields reported by Janechek et al. (2019). Under low-NO$_x$

175   conditions (Fig. 1a), SOA yields exhibited a slow growth, reaching a plateau after 10 equivalent days. This

176   may be due to increased gas-phase fragmentation of cVMS to generate some higher volatility products,

177   leading to a small increasing amplitude of partition ratio of species into SOA at longer photochemical ages.
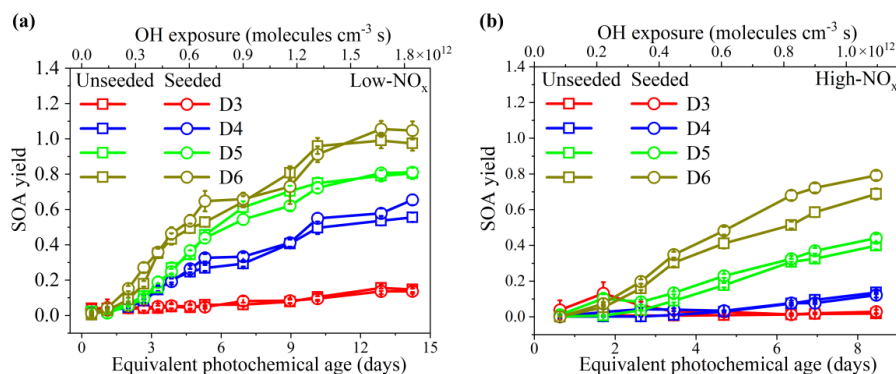
179   Figure 1. SOA yields from unseeded and seeded (30 µg m^{-3}) photooxidation of cVMS by OH radicals. **(a)**

180   low-NO$_x$ experiments; **(b)** high-NO$_x$ experiments.

182   For the unseeded and low-NO$_x$ experiments in Fig. 1a, SOA yields of four cVMS exhibited significant

183   differences in values over the same number of equivalent days. The SOA yields successively increased from

184   D3 to D6, consistent with the volatilities and molecular masses of the cVMS as well as their reaction rate

185   constants with the OH radical (Alton and Browne, 2020; Kim and Xu, 2017; Safron et al., 2015). The

186   maximum SOA yields of D3-D6 were (0.16±0.02), (0.56±0.03), (0.80±0.03) and (0.99±0.04), respectively,

187   occurring after a PA of 12 equivalent days. It has been reported that D5 SOA yields varied in the range of

188   0.08-0.50 (Janechek et al., 2019; Wu and Johnston, 2017). Under a similar OH exposure (1.6-1.7×10^{12}

189   molecules cm^{-3} s), the D5 SOA yield (0.79±0.03) obtained here is considerably higher than that (0.22)

190   measured by Janechek et al. (2019), which may be attributed to differences in experimental conditions such

191   as differences in wall losses, SOA measurement methods, RHs, and D5 concentrations (Table S2). Although

192   the amount of cVMS lost was variable, cVMS SOA yields positively depended on SOA mass concentrations

193   (Fig. S2), and this trend was observed in previous D5 SOA experiments with OH oxidation (Wu and Johnston,

194   2017).

195   As shown in Fig. 1b, the order of SOA yields from the four cVMS under high-NO_x conditions was the

196   same as that under low-NO_x conditions. However, the SOA yields under high-NO_x conditions were generally

197   smaller than the corresponding yields at similar OH exposures under low-NO_x conditions, with a decrease

198   of 0.05-0.30 depending on the cVMS. Such a reduction suggests that NO_x can restrict the formation of cVMS

199   SOA. NO_x has been shown to reduce SOA yields for some anthropogenic alkanes (Li et al., 2019b), aromatics

200   (Ng et al., 2007a; Chan et al., 2009; Zhou et al., 2019), monoterpenes (Zhao et al., 2018) and other terpenes

201   (Ng et al., 2007b), attributable to the formation of higher volatility products (e.g., organic nitrates) generated

202   by RO_2 + NO compared to RO_2 + HO_2 (Presto et al., 2005; Li et al., 2019b), which is also likely the case

203   here. The higher volatility products favor partitioning in the gas phase, thus reducing the potential for

204   forming SOA (Zhou et al., 2019). Moreover, high NO_x levels can suppress the formation of products for

205   nucleation, thereby reducing aerosol surface as a condensational sink and increasing the wall loss of

206   condensable species in an OFR under high-NO_x conditions (Zhao et al., 2018; Sarrafzadeh et al., 2016; Wildt

207   et al., 2014). Figure S3 indicates that the difference between SOA yields with and without NO_x decreased

208   with increasing silicon atoms within individual cVMS, indicating a less restricting effect of NO_x on the SOA

209   formation for larger cVMS. This means that high NO_x levels play a lessor role in the SOA yields of lower

210   volatility precursors.

211   SOA yields in the AS-seeded experiments under low and high-NO_x conditions are also shown in Figs. 1

212   and S3, indicating minimal impacts of the AS seed particles on SOA yields. A yield enhancement ratio

213   (R_E=Y_{seeded}/$Y_{unseeded}$, Fig. S4) was used to show the seed impacts more clearly. Under low-NO_x conditions,

214   the R_E values for all cVMS were close to 1.0 (Fig. S4a), suggesting negligible impact of AS seed particles

215   on SOA yields; however, under high-NO_x conditions, R_E was much larger (17.81, 13.18 and 15.51 for D3-

216   D5, respectively) at short PA but gradually decreased to 1.0 with increasing PA for D3-D5, while it was

217   always close to 1.0 for D6 regardless of PA (Fig. S4b). R_E values greater than 1.0 suggest that AS seed

218   particles played an enhancement role in the cVMS SOA formation, as similarly reported in SOA formation

219   from hydrocarbons (Sarrafzadeh et al., 2016; Lamkaddam et al., 2017; Li et al., 2019b). Under low-NO_x

220   conditions, the general lack of impact on cVMS SOA yields by the AS seed particles suggests that

221   condensation was not the main process driving SOA formation in cVMS oxidation. For the few cases of high

222   NO_x level at low PA, where R_E was >1 for D3-D5, it is possible that their early generations of oxidation

223   products were more volatile than successive generations of products and hence more prone to condensation

224   enhanced by AS seeds. As PA increased, further reactions of these early generation oxidation products with

225   OH radicals resulted in further generation products that were likely less volatile, thereby weakening the

226   enhancing role of AS seeds at high OH exposure. Such effect was less pronounced for D6, likely because its

227   oxidation products at different PA had similar volatilities. Figure S4b shows that the effect of AS seed

228   particles on SOA yields negatively correlated with the number of silicon atoms in the cVMS. Lower volatility

229   precursors (D5 and D6) formed lower volatile products (Alton and Browne, 2020), resulting in SOA yields

230   less sensitive to the pre-existing seeds. In fact, the oxidation products of D5 have been shown to be nearly

231   non-volatile (Janechek et al., 2019; Wu and Johnston, 2017).

232   **3.2 Aerosol compositions**

233   **3.2.1 Compositions of SOA under low-NO_x conditions.**

234   Figures 2 and S5 show the normalized HR-ToF-AMS mass spectra of cVMS SOA from unseeded

235   experiments under low-NO_x conditions at OH exposures of 9.0×10^{11} molecules cm^{-3} s. The mass spectral

236   signals can be identified as fragments with a formula of $C_xH_yO_zSi_n$. For D3 SOA, the most prominent peaks

237   were at m/z 44 and 29, dominated by CO_2^+ and CHO^+, which were tracers for organic acids (Ng et al., 2010),

238   alcohols and aldehydes (Lee et al., 2012), respectively. They may result from the oxidation of the methyl

239   groups in D3 by OH radicals. For the mass spectra of D4-D6 SOA, the two highest peaks at m/z 14 and 15

240   were CH_2^+ and CH_3^+, respectively. In addition, there were several dominant $C_xH_yO_zSi_n$ peaks, which were

241   fragments of silicon-containing products. For the $C_xH_yO_zSi_n$ group in D4 SOA, there were four typical peaks

242   at m/z 255, 257, 271 and 273, with formulae of $C_4H_{11}O_7Si_3^+$, $C_3H_9O_8Si_3^+$, $C_3H_7O_9Si_3^+$ and $C_3H_9O_9Si_3^+$,

243   respectively. The $C_xH_yO_zSi_n$ fragment group containing Si of D5 SOA had three dominant peaks at m/z 327,

244   329 and 331, corresponding to $C_{12}H_{11}O_2Si_5^+$, $C_9H_9O_8Si_3^+$ and $C_5H_{15}O_9Si_4^+$, respectively. For the $C_xH_yO_zSi_n$

245   group containing Si in D6 SOA, there were five main peaks at m/z 73 (C_3H_9Si), 387 ($C_8H_{23}O_8Si_5^+$), 389

246   ($C_8H_9O_9Si_5^+$), 401 ($C_9H_{21}O_{10}Si_4^+$) and 403 ($C_7H_{15}O_{12}Si_4^+$).

247

248
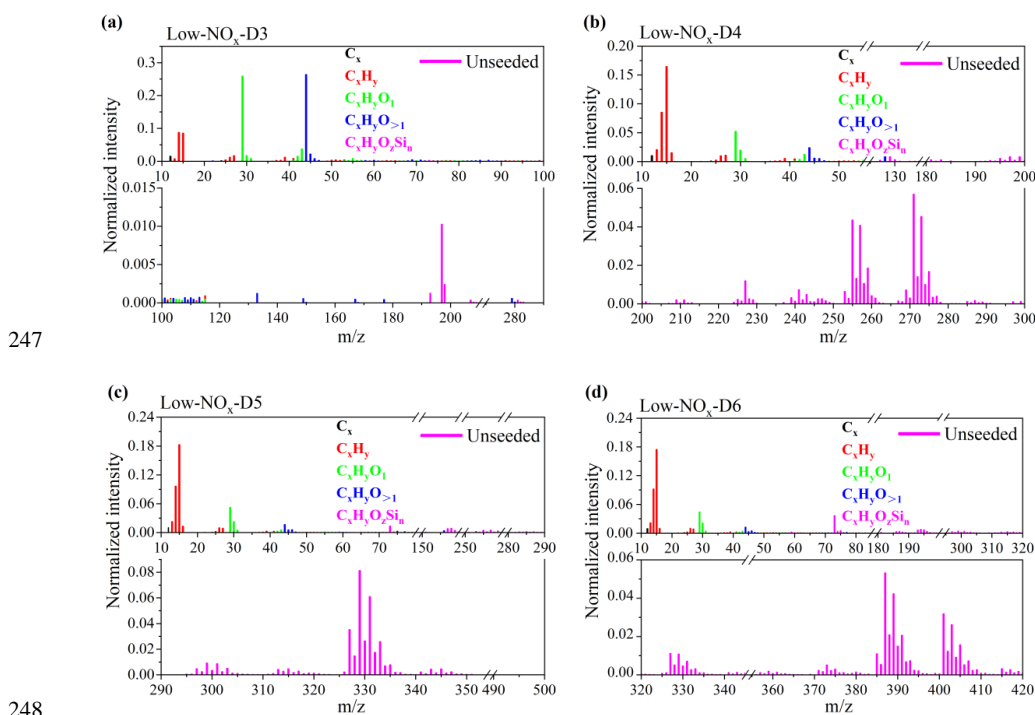
Figure 2. HR-ToF-AMS mass spectra of cVMS SOA at OH exposure of 9.0×10^{11} molecules cm^{-3} s under

low-NO$_x$ conditions in unseeded experiments. **a-d** represent the mass spectra of D3-D6 SOA, respectively.

251

252   Figure 3 shows the evolution of different groups of ions in the HR-ToF-AMS spectra of the cVMS SOA

253   as a function of PA in equivalent days. For D3-D6 under unseeded conditions, $C_xH_yO_1$ and $C_xH_yO_{>1}$ ions

254   significantly decreased within 0-4 equivalent days of PA, but remained essentially unchanged when PA

255   increased to 7-15 equivalent days. The C_xH_y ion increased to its peak value at about 9 equivalent days of PA

256   for D3 and 2-3 equivalent days of PA for D4-D6, and then gradually decreased with further PA increases.

257   The $C_xH_yO_zSi_n$ group of ions maintained an increasing trend until 9-10 days of PA, thereafter it decreased

258   slightly for D4-D6 SOA. The weighted values of the atomic number ratios Si/C (n/x) and Si/O (n/z) for the

259   $C_xH_yO_zSi_n$ groups in D5 and D6 SOA at different PA are plotted in Fig. S6, which can be used to indicate

260   the changes in the Si element of SOA. The n/x ratio at initial SOA formation stage was close to that (0.50)

261   in D5 and D6 molecules, and then increased continuously with increasing PA. The n/z ratio kept increasing

262   from 0.53 to 1.15 for D5 SOA and from 0.72 to 1.32 for D6 SOA, but varying around 1.0 that was the Si/O

263   ratio in D5 and D6. While it is difficult to separate the effect of fragmentation due to the AMS ionization

264   process, the relative changes of group intensities and the evolution of n/x and n/z in $C_xH_yO_zSi_n$ over different

265   PA may be attributed to the initial substitution of methyl groups on the -Si-O- ring of the cVMS by OH or

266   CH_2OH when oxidized by the OH radicals (Wu and Johnston, 2016; Alton and Browne, 2020). Si-containing

267   products such as silanols may partition into SOA and result in an appearance of $C_xH_yO_zSi_n$ ions in the AMS

268   mass spectra. It is possible that in this process, the Si-O bonds may continue to be cleaved from OH radical

269   attack, followed by further deposition of less volatile and nonvolatile products containing $C_xH_yO_zSi_n$ on the

270   SOA.
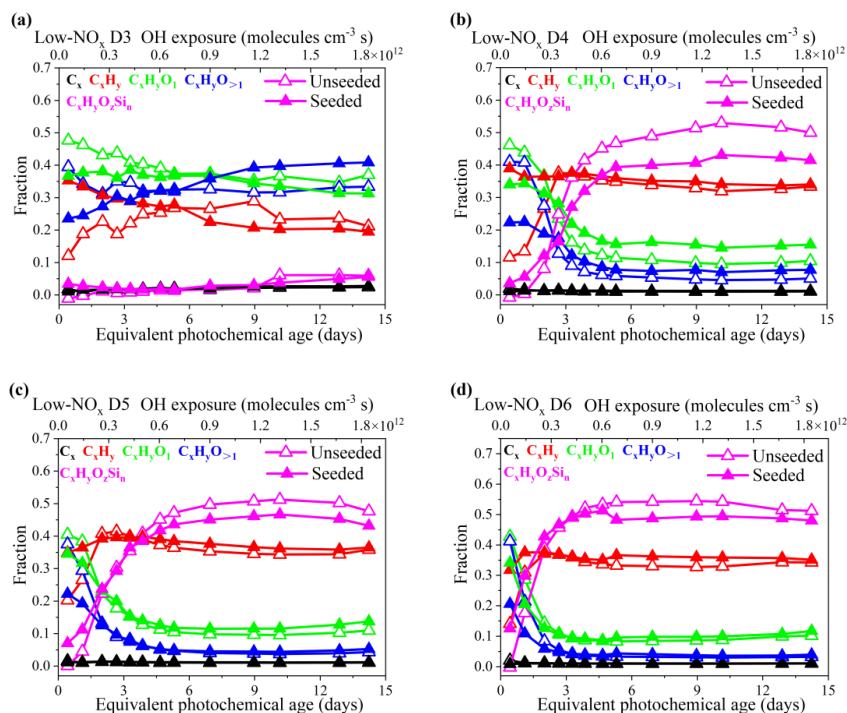
Figure 3. Fraction of C_x, C_xH_y, $C_xH_yO_1$, $C_xH_yO_{>1}$ and $C_xH_yO_zSi_n$ ion groups for SOA derived from the oxidation of cVMS (**a-d**) by OH radicals at different photochemical ages under low-NO_x conditions. Empty and solid triangles represent experimental data under unseeded and seeded conditions, respectively.

As shown in Fig. 3, the presence of seeds led to some changes in the evolution trends of ion groups in the AMS spectra. For instance, the initial fraction of C_xH_y in seeded experiments was larger than that in unseeded experiments, whereas $C_xH_yO_1$ and $C_xH_yO_{>1}$ exhibited opposite changes. The presence of seeds led to larger initial and smaller steady-state $C_xH_yO_zSi_n$ fractions than those in unseeded experiments. Regardless of the presence of seeds, C_xH_y, $C_xH_yO_1$ and $C_xH_yO_{>1}$ mainly contributed to the composition of all cVMS SOA at initial OH radicals oxidation, but D4-D6 SOA primarily consisted of C_xH_y and $C_xH_yO_zSi_n$ after 6 equivalent days.

284   **3.2.2 Compositions of SOA under high-NO$_x$ conditions.**

285   Figure S7 shows the HR-ToF-AMS mass spectra of cVMS SOA under high-NO$_x$ conditions at OH

286   exposures of 9.0×10^{11} molecules cm^{-3} s (-6.9 d). Compared to that under low-NO$_x$ conditions (Figs. 2 and

287   S5), there was one additional N-containing group (N$_m$O$_z$) in the SOA mass spectra under high-NO$_x$

288   conditions, which accounted for 16%-31%. For the mass spectra of D3-D6 SOA originating from unseeded

289   experiments under high-NO$_x$ conditions in Fig. S7, the dominating peaks of the N$_m$O$_z$ family were m/z 30

290   (NO$^+$) and m/z 46 (NO$_2^+$). The common main peaks were located at m/z 30 (NO$^+$) for cVMS SOA, m/z 44

291   (CO$_2^+$) for D3-D4 SOA, and m/z 46 (NO$_2^+$) for D4-D6 SOA. In addition, there were other primary peaks at

292   m/z 29 (CHO$^+$) for D4 SOA, while m/z 15 (CH$_3^+$) and m/z 28 (CO$^+$) for D5-D6 SOA. The m/z 28 (CO$^+$),

293   similar with m/z 44 (CO$_2^+$), is considered as a tracer for organic acids (Ng et al., 2010). In the mass spectra

294   for D3-D6 SOA under high-NO$_x$ conditions, the presence of NO$^+$ (m/z 30) and NO$_2^+$ (m/z 46) illustrated the

295   formation of nitrates in SOA (Ng et al., 2007b).

296   For the C$_x$H$_y$O$_z$Si$_n$ group in the D4 SOA mass spectrum under high-NO$_x$ conditions, the dominating peaks

297   and their formulas were same as those under low-NO$_x$ conditions. For the C$_x$H$_y$O$_z$Si$_n$ group in D5 SOA, in

298   addition to two typical peaks at m/z 327 and 329 in the low-NO$_x$ experiments, there was another prominent

299   peak at m/z 328, with a formula C$_8$H$_{12}$O$_5$Si$_5$. The C$_x$H$_y$O$_z$Si$_n$ group in D6 SOA had three typical peaks at m/z

300   73 (C$_3$H$_9$Si), m/z 387 (C$_8$H$_{23}$O$_8$Si$_5^+$) and m/z 401 (C$_9$H$_{21}$O$_{10}$Si$_4^+$). For the C$_x$H$_y$O$_z$Si$_n$ groups in cVMS SOA,

301   there was little difference in the x, y, z and n value assignment of C$_x$H$_y$O$_z$Si$_n$ peaks in SOA generated under

302   low-NO$_x$ and high-NO$_x$ conditions, suggesting the formation of similar Si-containing oxidation products.

303   For cVMS SOA under high-NO$_x$ conditions, the evolution of family groups as a function of OH exposure

304   was summarized in Fig. S8. The dominated composition at initial stage was C$_x$H$_y$O$_{>1}$ groups for D3-D6 SOA.

305   At equivalent days larger than 6, D3 SOA primarily consisted of C$_x$H$_y$O$_{>1}$, N$_m$O$_z$ and C$_x$H$_y$O$_1$ groups, while

306 D4-D6 SOA was mainly composed of $C_xH_yO_zSi_n$, N_mO_z, $C_xH_yO_1$, C_xH_y and $C_xH_yO_{>1}$ groups. Figure S8 also

307 shows influences of seeds on the evolution of family groups under high-NO_x conditions. It was observed

308 that all groups in D3-D6 SOA displayed similar change trends regardless of the existence of seeds. As shown

309 in Fig. S9, the trend of the weighted values of the atomic ratio n/z in the $C_xH_yO_zSi_n$ groups at different

310 photochemical ages under high-NO_x conditions was similar to that in low-NO_x experiments. However, the

311 n/x ratios remained almost unchanged, and were close to the initial value (0.5) in cVMS. This may be

312 attributed to possible suppression of cleavage of methyl groups from the -Si-O- ring of the cVMS under

313 high-NO_x conditions.

4 Conclusions and implications

315   The yields and compositions of SOA generated from the photooxidation of four cVMS (D3-D6) with OH

316 radicals were investigated using an oxidation flow reactor. cVMS SOA yields exhibited an overall increasing

317 trend with PA, and their values gradually increased with cVMS from D3 to D6. SOA formations depended

318 on NO_x, as shown by smaller SOA yields under high-NO_x conditions. Ammonium sulfate seeds significantly

319 enhanced SOA yields of D3-D5 at short PA under high-NO_x conditions. The SOA mass spectra showed that

320 Si-containing species were one of main chemical compositions at PA of >6 days.

321   To evaluate the potential contributions of cVMS to SOA formation in the atmosphere, global SOA

322 concentrations produced from cVMS were estimated according to the cVMS SOA yields measured in this

323 work and using the cVMS concentrations reported from multiple studies, which were listed in Table S3.

324 Here, under the seeded conditions, the high-NO_x SOA yields at 8.5 equivalent days (D3: 0.028; D4: 0.122;

325 D5: 0.441; D6: 0.792) are employed in the calculation of cVMS SOA concentrations at urban sites, while

326 the low-NO_x SOA yields under the unseeded conditions at 14.2 equivalent days (D3: 0.148; D4: 0.556; D5:

327 0.805; D6: 0.975) are used to estimate cVMS SOA at background and polar sites. Figure 4 shows the global

328   concentration distribution of SOA from four cVMS (D3-D6) at 36 sites worldwide estimated by the Equation

329   4,

330
$$C_{\text{cVMS-SOA}} = C_{\text{cVMS}} \times \frac{\Delta C_{\text{cVMS}}}{C_{\text{in-cVMS}}} \times Y \qquad (4)$$

331   where C_{cVMS} and $C_{\text{cVMS-SOA}}$ are the mass concentration of cVMS reported from literatures and cVMS SOA

332   estimated in global sites, respectively; $C_{\text{in-cVMS}}$ and ΔC_{cVMS} are the mass concentration of initial and lost

333   cVMS at the selected equivalent days during the experiments of this work, respectively; Y is the cVMS SOA

334   mass yields mentioned above. Table S3 summarizes the details regarding sites and concentrations of cVMS

335   SOA. The derived concentrations of cVMS SOA varies significantly among urban, background and polar

336   sites. The total cVMS SOA concentrations in urban areas are the highest, up to 1249 ng/m^3. They are 14.5-

337   347 and 10.5-105.3 ng/m^3 for background and Arctic sites, respectively. cVMS SOA concentrations in urban

338   regions of Asia (sites 29-36) and Europe (sites 26-28) are generally larger than that of North America (sites

339   20-25). In China, the total cVMS SOA concentrations in urban sites range from 14.7 to 1249 ng/m^3. The

340   main precursors of cVMS SOA are different among Chinese cities. For three cities along the southeast coast

341   of China (Guangzhou, Macau and Foshan), the dominant precursors of cVMS SOA are D3 and D4, which

342   are related to industrial emissions of these two siloxanes in this region (Wang et al., 2001). For Dalian in

343   China, mainly D5 and D6 contribute to cVMS SOA, which have the highest concentrations among all sites.

344   This can be attributed to the industrial production of D5 and D6 and the use of personal care products in

345   Dalian (Li et al., 2020). In the other Chinese urban areas with reported cVMS concentrations (Lhasa, Golmud,

346   Kunming and Yantai), the total cVMS SOA concentrations are considerably smaller than those in the urban

347   areas above, with D5 acting as the main precursor, which may be ascribed to the relatively low population

348   densities in these cities (Wang et al., 2018).
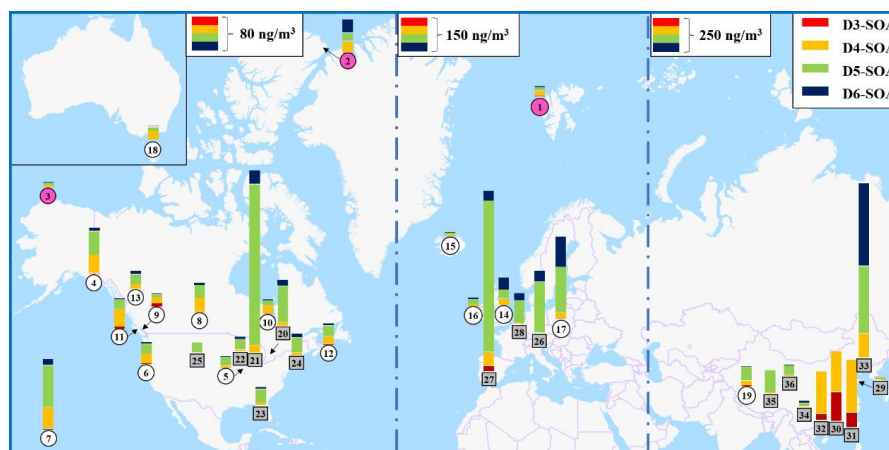
349

350   Figure 4. Global concentrations of cVMS SOA (ng/m³) on the basis of the cVMS concentrations

351   reported from multiple studies and the cVMS SOA yields measured in this work. The numbers of polar,

352   background and urban sites are enclosed in pink, white circles and gray boxes, respectively. The details

353   about cVMS and SOA concentrations at different sites were summarized in Table S3 of Supplement.

354

355   At urban sites in Europe and North America, cVMS SOA concentrations are reported in the range of 131-

356   773 ng/m³ and 21.8-416 ng/m³, respectively. Among these cVMS, D5 is the main contributor to cVMS SOA

357   at these locations, averaging 80.4% of total cVMS SOA. This contribution is higher than that (73.9%) at

358   Chinese urban sites. For instance, D5 SOA is calculated to be 652 ng/m³ in Catalan, Spain, 369 ng/m³ in

359   Chicago, USA, 218 ng/m³ in Zurich, Switzerland and 94 ng/m³ in Paris, France, where there are high levels

360   of economic activities and high population densities. These results suggest that personal care products as a

361   main source of D5 may be the most important anthropogenic origins of Si-containing SOA in Europe and

362   North America.

363   At background and Arctic sites, cVMS SOA are primarily derived from D4 and D5. The background sites

364   are located in mountains, rural areas, forested areas, lakes and at high altitudes. The three highest cVMS

18

365   SOA concentrations at background sites are located at Kosetice in the Czech Republic (347 ng/m^3), Hilo,

366   Hawaii, USA (157 ng/m^3) and Tibetan Plateau in China (134 ng/m^3), where the contribution percentages of

367   SOA from both D4 and D5 are 61.9%, 90.3% and 94.9%, respectively. The cVMS SOA concentrations at

368   the Little Fox Lake site in Yukon, Canada is the highest (105.3 ng/m^3) among the four locations in the Arctic,

369   91% of which is accounted for by both D4 and D5 SOA. The dominance of D4 and D5 SOA in both

370   background and the Arctic regions highlights their persistence in atmosphere and the potential for long-range

371   atmospheric transport.

372   Furthermore, global concentration distribution of Si-containing SOA estimated for the four cVMS (D3-

373   D6) at 36 sites worldwide is also presented in Table S3, which clearly shows the global importance of Si in

374   SOA with the estimated percentages of cVMS SOA that contains the Si element. For example, up to 49.6%

375   and 31.2% of cVMS SOA contained Si elements in background and urban sites, respectively. These results

376   are similar to the summary observations that reported percentages of aerosols with a Si mole fraction >0.01

377   (%) at different sites (Bzdek et al., 2014). The above results demonstrated that Si is a frequent component of

378   SOA in background and urban areas.

379   The global annual production of D4, D5 and D6 is about 1, 0.1 and 0.01 Tg·yr^{-1}, respectively, and 90% of

380   these cVMS is eventually released into the atmosphere (Li et al., 2020; Genualdi et al., 2011; Wang et al.,

381   2013; Sakurai et al., 2019). Based on the results shown in Fig. 4, the annual production of cVMS (D4-D6)

382   SOA was estimated to be 0.16 Tg·yr^{-1}, which was about 5.5% of SOA (2.9 Tg·yr^{-1}) produced from mobile

383   source emissions in the USA and 5-8 times of SOA generated by Athabasca oil sands (0.02-0.03 Tg·yr^{-1}, one

384   of the largest sources of anthropogenic secondary organic aerosols in North America) (Tkacik et al., 2014;

385   Liggio et al., 2016). Moreover, it was also 0.8% and 2.3% of isoprene-SOA (20 Tg·yr^{-1}) and monoterpenes-

386   SOA (7 Tg·yr^{-1}) (typical biogenic SOA), respectively, indicating the potential importance of cVMS SOA

Atmospheric
Chemistry
and Physics
Discussions

387 (Jokinen et al., 2015). While these cVMS SOA sources may seem small, they can make substantially higher

388 contributions to ambient air SOAs in population centers where cVMS compounds are primarily used.

389

390 **Author contributions**

391 CH designed and conducted all experiments; CH and HY analyzed the data and prepared the paper with

392 contributions from KL, PL, JL, AL and SML. SML supervised the project.

393

394 **Competing interests**

395 The authors declare that they have no conflict of interest.

396 **Acknowledgements**

401

402 **References**

403 Ahrens, L., Harner, T., and Shoeib, M.: Temporal Variations of Cyclic and Linear Volatile Methylsiloxanes in the

404 Atmosphere Using Passive Samplers and High-Volume Air Samplers, Environ. Sci. Technol., 48, 9374-9381,

405 https://doi.org/10.1021/es502081j, 2014.

406 Allen, R., Kochs, P., and Chandra, G.: Industrial Organosilicon Materials, Their Environmental Entry and

407 Predicted Fate, Springer, 3, 1-25, https://doi.org/10.1007/978-3-540-68331-5_1, 1997.

408 Alton, M. and Browne, E.: Atmospheric Chemistry of Volatile Methyl Siloxanes: Kinetics and Products of

409 Oxidation by OH Radicals and Cl Atoms, Environ. Sci. Technol., 54, 5992-5999,

410 https://dx.doi.org/10.1021/acs.est.0c01368, 2020.

411   Atkinson, R.: Kinetics of the Gas-Phase Reactions of a Series of Organosilicon Compounds with OH and NO_3

412   Radicals and O_3 at 297 ± 2 K, Environ. Sci. Technol., 25, 863-866, https://doi.org/10.1021/es00017a005, 1991.

413   Bein, K., Zhao, Y., Wexler, A., Johnston, M.: Speciation of Size-Resolved Individual Ultrafine Particles in

414   Pittsburgh, Pennsylvania, J. Geophys. Res., 110, D07S05, https://doi.org/10.1029/2004jd004708, 2005.

415   Berndt, T., Richters, S., Jokinen, T., Hyttinen, N., Kurtén, T., Otkjaer, R., Kjaergaard, H., Stratmann, F., Herrmann,

416   H., Sipilä, M., Kulmala, M., and Ehn, M.: Hydroxyl Radical-Induced Formation of Highly Oxidized Organic

417   Compounds, Nat. Commun., 7, 1-8, https://doi.org/10.1038/ncomms13677, 2016.

418   Bruns, E., Haddad, I., Keller, A., Klein, F., Kumar, N., Pieber, S., Corbin, J., Slowik, J., Brune, W., Baltensperger,

419   U., and Prévôt, A.: Inter-Comparison of Laboratory Smog Chamber and Flow Reactor Systems on Organic

420   Aerosol Yield and Composition, Atmos. Meas. Tech., 8, 2315-2332, https://doi.org/10.5194/amt-8-2315-2015,

421   2015.

422   Bzdek, B., Horan, A., Pennington, M., Janechek, N., Baek, J., Stanier, C., and Johnston, M.: Silicon is a Frequent

423   Component   of   Atmospheric   Nanoparticles,   Environ.   Sci.   Technol.,   48,   11137-11145,

424   https://doi.org/10.1021/es5026933, 2014.

425   Chan, A., Kautzman, K., Chhabra, P., Surratt, J., Chan, M., Crounse, J., Kürten, A., Wennberg, P., Flagan, R., and

426   Seinfeld, J.: Secondary Organic Aerosol Formation from Photooxidation of Naphthalene and Alkylnaphthalenes:

427   Implications for Oxidation of Intermediate Volatility Organic Compounds (IVOCs), Atmos. Chem. Phys., 9,

428   3049–3060, https://doi.org/10.5194/acp-9-3049-2009, 2009.

429   Chandramouli, B., Kamens, R.: The Photochemical Formation and Gas-Particle Partitioning of Oxidation

430   Products of Decamethyl Cyclopentasiloxane and Decamethyl Tetrasiloxane in the Atmosphere, Atmos.

431   Environ., 35, 87-95, https://doi.org/10.1016/S1352-2310(00)00289-2, 2001.

432   Charan, S., Huang, Y., Buenconsejo, R., Li, Q., Cocker III, D., and Seinfeld, J.: Secondary Organic Aerosol

433   Formation   from   the   Oxidation   of   Decamethylcyclopentasiloxane   at   Atmospherically   Relevant   OH

434   Concentrations, Atmos. Chem. Phys., https://doi.org/10.5194/acp-2021-353, 2021.

435   Coggon, M., McDonald, B., Vlasenko, A., Veres, P., Bernard, F., Koss, A., Yuan, B., Gilman, J., Peischl, J., Aikin,

436   K., DuRant, J., Warneke, C., Li, S.-M., and Gouw, J.: Diurnal Variability and Emission Pattern of

437   Decamethylcyclopentasiloxane (D5) from the Application of Personal Care Products in Two North American

438   Cities, Environ. Sci. Technol., 52, 5610-5618, https://doi.org/10.1021/acs.est.8b00506, 2018.

439   Farasani, A. and Darbre, P.: Exposure to Cyclic Volatile Methylsiloxanes (cVMS) Causes Anchorage-Independent

440   Growth and Reduction of BRCA1 in Non-Transformed Human Breast Epithelial Cells, J. Appl. Toxicol., 37,

441   454-461, https://doi.org/10.1002/jat.3378, 2017.

442   Genualdi, S., Harner, T., Cheng, Y., Macleod, M., Hansen, K., Egmond, R., Shoeib, M., and Lee, S.: Global

443   Distribution of Linear and Cyclic Volatile Methyl Siloxanes in Air, Environ. Sci. Technol., 45, 3349-3354,

444   https://doi.org/10.1021/es200301j, 2011.

445   Glasius, M. and Goldstein, A.: Recent Discoveries and Future Challenges in Atmospheric Organic Chemistry,

446   Environ. Sci. Technol., 50, 2754-2764, https://doi.org/10.1021/acs.est.5b05105, 2016.

447   Guo, J., Zhou, Y., Cui, J., Zhang, B., and Zhang, J.: Assessment of Volatile Methylsiloxanes in Environmental

448   Matrices   and   Human   Plasma,   Sci.   Total.   Environ.,   668,   1175-1182,

449   https://doi.org/10.1016/j.scitotenv.2019.03.092, 2019.

450   Huang, Y., Coggon, M., Zhao, R., Lignell, H., Bauer, M., Flagan, R., and Seinfeld, J.: The Caltech Photooxidation

451   Flow Tube reactor: Design, Fluid Dynamics and Characterization, Atmos. Meas. Tech., 10, 839-867,

452   https://doi.org/10.5194/amt-10-839-2017, 2017.

453   Janechek, N., Hansen, K., and Stanier, C.: Comprehensive Atmospheric Modeling of Reactive Cyclic Siloxanes

454   and their Oxidation Products, Atmos. Chem. Phys., 17, 8357-8370, https://doi.org/10.5194/acp-17-8357-2017,

455   2017.

456   Janechek, N., Marek, R., Bryngelson, N., Singh, A., Bullard, R., Brune, W., and Stanier, C.: Physical Properties

457   of Secondary Photochemical Aerosol from OH Oxidation of a Cyclic Siloxane, Atmos. Chem. Phys., 19, 1649-

458   1664, https://doi.org/10.5194/acp-19-1649-2019, 2019.

459   Jokinen, T., Berndt, T., Makkonen, R., Kerminen, V., Junninen, H., Paasonen, P., Stratmann, F., Herrmann, H.,

460   Guenther, A., Worsnop, D., Kulmala, M., Ehn, M., and Sipilä, M.: Production of Extremely Low Volatile

461   Organic Compounds from Biogenic Emissions: Measured Yields and Atmospheric Implications, Proc. Natl.

462   Acad. Sci. U S A., 112, 7123-7128, https://doi.org/10.1073/pnas.1423977112, 2015.

463   Kierkegaard, A. and McLachlan, M.: Determination of Linear and Cyclic Volatile Methylsiloxanes in Air at a

464   Regional   Background   Site   in   Sweden,   Atmos.   Environ.,   80,   322-329,

465   https://doi.org/10.1016/j.atmosenv.2013.08.001, 2013.

466   Kim, J. and Xu, S.: Quantitative Structure-Reactivity Relationships of Hydroxyl Radical Rate Constants for Linear

467   and Cyclic Volatile Methylsiloxanes, Environ. Toxicol. Chem., 36, 3240-3245, https://doi.org/10.1002/etc.3914,

468   2017.

469   Kim, J., Mackay, D., and Whelan, M.: Predicted Persistence and Response Times of Linear and Cyclic Volatile

470   Methylsiloxanes   in   Global   and   Local   Environments,   Chemosphere,   195,   325-335,

471   https://doi.org/10.1016/j.chemosphere.2017.12.071, 2018.

472   Krogseth, I., Zhang, X., Lei, Y., Wania, F., and Breivik, K.: Calibration and Application of a Passive Air Sampler

473   (XAD-PAS) for Volatile Methyl Siloxanes, Environ. Sci. Technol., 47, 4463-4470,

474   https://doi.org/10.1021/es400427h, 2013a.

475   Krogseth, I., Kierkegaard, A., McLachlan, M., Breivik, K., Hansen, K., and Schlabach, M.: Occurrence and

476   Seasonality of Cyclic Volatile Methyl Siloxanes in Arctic Air, Environ. Sci. Technol., 47, 502-509,

477   https://doi.org/10.1021/es3040208, 2013b.

478   Lambe, A., Chhabra, P., Onasch, T., Brune, W., Hunter, J., Kroll, J., Cummings, M., Brogan, J., Parmar, Y.,

479   Worsnop, D., Kolb, C., and Davidovits, P.: Effect of Oxidant Concentration, Exposure Time, and Seed Particles

480   on Secondary Organic Aerosol Chemical Composition and Yield, Atmos. Chem. Phys., 15, 3063-3075,

481   https://doi.org/10.5194/acp-15-3063-2015, 2015.

482   Lambe, A., Ahern, A., Williams, L., Slowik, J., Wong, J., Abbatt, J., Brune, W., Ng, N., Wright, J., Croasdale, D.,

483   Worsnop, D., Davidovits, P., and Onasch, T.: Characterization of Aerosol Photooxidation Flow Reactors:

484   Heterogeneous Oxidation, Secondary Organic Aerosol Formation and Cloud Condensation Nuclei Activity

485   Measurements, Atmos. Meas. Tech., 4, 445-461, https://doi.org/10.5194/amt-4-445-2011, 2011.

486   Lambe, A., Massoli, P., Zhang, X., Canagaratna, M., Nowak, J., Daube, C., Yan, C., Nie, W., Onasch, T., Jayne,

487   J., Kolb, C., Davidovits, P., Worsnop, D., and Brune, W.: Controlled Nitric Oxide Production via $O(^1D) + N_2O$

488   Reactions for Use in Oxidation Flow Reactor Studies, Atmos. Meas. Tech., 10, 2283-2298,

489   https://doi.org/10.5194/amt-10-2283-2017, 2017.

490   Lamkaddam, H., Gratien, A., Pangui, E., Cazaunau, M., Varrault, B., and Doussin, J.: High-NO_x Photooxidation

491   of n-Dodecane: Temperature Dependence of SOA Formation, Environ Sci Technol, 51, 192-201,

492   https://doi.org/10.1021/acs.est.6b03821, 2017.

493   Lee, A., Hayden, K., Herckes, P., Leaitch, W., Liggio, J., Macdonald, A., and Abbatt, J.: Characterization of

494   Aerosol and Cloud Water at a Mountain Site During WACS 2010: Secondary Organic Aerosol Formation

495   through Oxidative Cloud Processing, Atmos. Chem. Phys., 12, 7103-7116, https://doi.org/10.5194/acp-12-

496   7103-2012, 2012.

497   Li, K., Liggio, J., Lee, P., Han, C., Liu, Q., and Li, S.-M.: Secondary Organic Aerosol Formation from α-Pinene,

498   Alkanes, and Oil Sand-Related Precursors in a New Oxidation Flow Reactor, Atmos. Chem. Phys., 19, 9715-

499   9731, https://doi.org/10.5194/acp-19-9715-2019, 2019a.

500   Li, K., Liggio, J., Han, C., Liu, Q., Moussa, S., Lee, P., and Li, S.-M.: Understanding the Impact of High-NO_x

501   Conditions on the Formation of Secondary Organic Aerosol in the Photooxidation of Oil Sand-Related

502   Precursors, Environ. Sci. Technol., 53, 14420-14429, https://doi.org/10.1021/acs.est.9b05404, 2019b.

503   Li, Q., Lan, Y., Liu, Z., Wang, X., Wang, X., Hu, J., and Geng, H.: Cyclic Volatile Methylsiloxanes (cVMSs) in

504   the Air of the Wastewater Treatment Plants in Dalian, China-Levels, Emissions, and Trends, Chemosphere, 256,

505   1-8, https://doi.org/10.1016/j.chemosphere.2020.127064, 2020.

506   Li, S.-M. and Winchester, J.: Particle Size Distribution and Chemistry of Late Winter Arctic Aerosols, J. Geophys.

507   Res., 95, 13897-13908, https://doi.org/10.1029/J095iD09p13897, 1990.

508   Li, S.-M. and Winchester, J.: Aerosol Silicon and Associated Elements in the Arctic High and Mid-Troposphere,

509   Atmos. Environ., 27, 2907-2912, https://doi.org/10.1016/0960-1686(93)90322-P, 1993.

510   Liggio, J., Li, S.-M., Hayden, K., Taha, Y., Stroud, C., Darlington, A., Drollette, B., Gordon, M., Lee, P., Liu, P.,

511   Leithead, A., Moussa, S., Wang, D., Brien, J., Mittermeier, R., Brook, J., Lu, G., Staebler, R., Han, Y., Tokarek,

512   T., Osthoff, H., Makar, P., Zhang, J., Plata, D., and Gentner, D.: Oil Sands Operations as a Large Source of

513   Secondary Organic Aerosols, Nature, 534, 91-94, https://doi.org/10.1038/nature17646, 2016.

514   Liu, N., Xu, L., and Cai, Y.: Methyl Siloxanes in Barbershops and Residence Indoor Dust and the Implication for

515   Human Exposures, Sci. Total. Environ., 618, 1324-1330, https://doi.org/10.1016/j.scitotenv.2017.09.250, 2018.

516   MacLeod, M., Kierkegaard, A., Genualdi, S., Harner, T., and Scheringer, M.: Junge Relationships in Measurement

517   Data   for   Cyclic   Siloxanes   in   Air,   Chemosphere,   93,   830-834,

518   https://doi.org/10.1016/j.chemosphere.2012.10.055, 2013.

519   Mao, J., Ren, X., Brune, W., Olson, J., Crawford, J., Fried, A., Huey, L., Cohen, R., Heikes, B., Singh, H., Blake,

520   D., Sachse, G., Diskin, G., Hall, S., and Shetter, R.: Airborne Measurement of OH Reactivity during INTEX-

521   B, Atmos. Chem. Phys., 9, 163-173, https://doi.org/10.5194/acp-9-163-2009, 2009.

522   McFiggans, G., Mentel, T., Wildt, J., Pullinen, I., Kang, S., Kleist, E., Schmitt, S., Springer, M., Tillmann, R., Wu,

523   C., Zhao, D., Hallquist, M., Faxon, C., Breton, M., Hallquist, A., Simpson, D., Bergström, R., Jenkin, M., Ehn,

524   M., Thornton, J., Alfarra, M., Bannan, T., Percival, C., Priestley, M., Topping, D., and Scharr, A.: Secondary

525   Organic   Aerosol   Reduced   by   Mixture   of   Atmospheric   Vapours,   Nature,   565,   587-593,

526   https://doi.org/10.1038/s41586-018-0871-y, 2019.

527   Ng, N., Kroll, J., Chan, A., Chhabra, P., Flagan, R., and Seinfeld, J.: Secondary Organic Aerosol Formation from

528   m-Xylene, Toluene, and Benzene, Atmos. Chem. Phys., 7, 3909–3922, https://doi.org/10.5194/acp-7-3909-

529   2007, 2007a.

530   Ng, N., Chhabra, P., Chan, A., Surratt, J., Kroll, J., Kwan, A., McCabe, D., Wennberg, P., Sorooshian, A., Murphy,

531 S., Dalleska, N., Flagan, R., and Seinfeld, J.: Effect of NO_x Level on Secondary Organic Aerosol (SOA)

532 Formation from the Photooxidation of Terpenes, Atmos. Chem. Phys., 7, 5159–5174,

533 https://doi.org/10.5194/acp-7-5159-2007, 2007b.

534 Ng, N., Canagaratna, M., Zhang, Q., Jimenez, J., Tian, J., Ulbrich, I., Kroll, J., Docherty, K., Chhabra, P., Bahreini,

535 R., Murphy, S., Seinfeld, J., Hildebrandt, L., Donahue, N., DeCarlo, P., Lanz, V., Prévôt, A., Dinar, E., Rudich,

536 Y., and Worsnop, D.: Organic Aerosol Components Observed in Northern Hemispheric Datasets from Aerosol

537 Mass Spectrometry, Atmos. Chem. Phys., 10, 4625-4641, https://doi.org/10.5194/acp-10-4625-2010, 2010.

538 Peng, Z., Taylor, J., Orlando, J., Tyndall, G., and Jimenez, J.: Organic Peroxy Radical Chemistry in Oxidation

539 Flow Reactors and Environmental Chambers and their Atmospheric Relevance, Atmos. Chem. Phys., 19, 813-

540 834, https://doi.org/10.5194/acp-19-813-2019, 2019.

541 Peng, Z., Palm, B., Day, D., Talukdar, R., Hu, W., Lambe, A., Brune, W., and Jimenez, J.: Model Evaluation of

542 New Techniques for Maintaining High-NO Conditions in Oxidation Flow Reactors for the Study of OH-

543 Initiated Atmospheric Chemistry, ACS. Earth. Space. Chem. , 2, 72-86,

544 https://doi.org/10.1021/acsearthspacechem.7b00070, 2017.

545 Phares, D., Rhoads, K., Johnston, M., and Wexler, A.: Size-Resolved Ultrafine Particle Composition Analysis 2.

546 Houston, J. Geophys. Res., 108, 1-14, https://doi.org/10.1029/2001jd001212, 2003.

547 Presto, A., Hartz, K., and Donahue, N.: Secondary Organic Aerosol Production from Terpene Ozonolysis. 2. Effect

548 of NO_x Concentration, Environ. Sci. Technol. , 39, 7046-7054, https://doi.org/10.1021/es050400s, 2005.

549 Rauert, C., Shoieb, M., Schuster, J., Eng, A., and Harner, T.: Atmospheric Concentrations and Trends of Poly- and

550 Perfluoroalkyl Substances (PFAS) and Volatile Methyl Siloxanes (VMS) over 7 Years of Sampling in the Global

551 Atmospheric Passive Sampling (GAPS) Network, Environ. Pollut., 238, 94-102,

552 https://doi.org/10.1016/j.envpol.2018.03.017, 2018.

553 Rhoads, K., Phares, D., Wexler, A., Johnston, M.: Size-Resolved Ultrafine Particle Composition Analysis 1.

554 Atlanta, J. Geophys. Res., 108, 1-13, https://doi.org/10.1029/2001jd001211, 2003.

555 Riipinen, I., Juuti, T., Pierce, J., Petäjä, T., Worsnop, D., Kulmala, M., and Donahue, N.: The Contribution of

556 Organics to Atmospheric Nanoparticle Growth, Nat. Geosci., 5, 453-458, https://doi.org/10.1038/ngeo1499,

557 2012.

558 Rücker, C. and Kümmerer, K.: Environmental Chemistry of Organosiloxanes, Chem. Rev., 115, 466-524,

559 https://doi.org/10.1021/cr500319v, 2015.

560 Safron, A., Strandell, M., Kierkegaard, A., and Macleod, M.: Rate Constants and Activation Energies for Gas-

561   Phase Reactions of Three Cyclic Volatile Methyl Siloxanes with the Hydroxyl Radical, Int. J. Chem. Kinet., 47,

562   420-428, https://doi.org/10.1002/kin.20919, 2015.

563   Sakurai, T., Imaizumi, Y., Kuroda, K., Hayashi, T., and Suzuki, N.: Georeferenced multimedia environmental fate

564   of volatile methylsiloxanes modeled in the populous Tokyo Bay catchment basin, Sci Total Environ, 689, 843-

565   853, https://doi.org/10.1016/j.scitotenv.2019.06.462, 2019.

566   Sarrafzadeh, M., Wildt, J., Pullinen, I., Springer, M., Kleist, E., Tillmann, R., Schmitt, S., Wu, C., Mentel, T., Zhao,

567   D., Hastie, D., and Scharr, A.: Impact of NO_x and OH on Secondary Organic Aerosol Formation from β-Pinene

568   Photooxidation, Atmos. Chem. Phys., 16, 11237-11248, https://doi.org/10.5194/acp-16-11237-2016, 2016.

569   Simonen, P., Saukko, E., Karjalainen, P., Timonen, H., Bloss, M., Saksa, P., Rönkkö, T., Keskinen, J., and Maso,

570   M.: A New Oxidation Flow Reactor for Measuring Secondary Aerosol Formation of Rapidly Changing

571   Emission Sources, Atmos. Meas. Tech., 10, 1519-1537, https://doi.org/10.5194/amt-10-1519-2017, 2017.

572   Sommerlade, R., Parlar, H., Wrobel, D , Kochs, P.: Product Analysis and Kinetics of the Gas-Phase Reactions of

573   Selected Organosilicon Compounds with OH Radicals Using a Smog Chamber-Mass Spectrometer System,

574   Environ. Sci. Technol., 27, 2435-2440, https://doi.org/10.1021/es00048a019, 1993.

575   Tang, X., Misztal, P., Nazaroff, W., and Goldstein, A.: Siloxanes Are the Most Abundant Volatile Organic

576   Compound Emitted from Engineering Students in a Classroom, Environ. Sci. Technol. Lett. , 2, 303-307,

577   https://doi.org/10.1021/acs.estlett.5b00256, 2015.

578   Tkacik, D., Lambe, A., Jathar, S., Li, X., Presto, A., Zhao, Y., Blake, D., Meinardi, S., Jayne, J., Croteau, P., and

579   Robinson, A.: Secondary Organic Aerosol Formation from in-Use Motor Vehicle Emissions Using a Potential

580   Aerosol Mass Reactor, Environ. Sci. Technol., 48, 11235-11242, https://doi.org/10.1021/es502239v, 2014.

581   Wang, D.-G., Norwood, W., Alaee, M., Byer, J., and Brimble, S.: Review of Recent Advances in Research on the

582   Toxicity, Detection, Occurrence and Fate of Cyclic Volatile Methyl Siloxanes in the Environment, Chemosphere,

583   93, 711-725, https://doi.org/10.1016/j.chemosphere.2012.10.041, 2013.

584   Wang, X., Schuster, J., Jones, K., and Gong, P.: Occurrence and Spatial Distribution of Neutral Perfluoroalkyl

585   Substances and Cyclic Volatile Methylsiloxanes in the Atmosphere of the Tibetan Plateau, Atmos. Chem. Phys.,

586   18, 8745-8755, https://doi.org/10.5194/acp-18-8745-2018, 2018.

587   Wang, X., Lee, S., Sheng, G., Chan, L., Fu, J., Li, X., Min, Y., and Chan, C.: Cyclic organosilicon compounds in

588   ambient air in Guangzhou, Macau and Nanhai, Pearl River Delta, Appl. Geochemistry, 16, 1447-1454,

589   https://doi.org/10.1016/S0883-2927(01)00044-0, 2001.

590   Whelan, M., Estrada, E., and Egmond, R.: A Modelling Assessment of the Atmospheric Fate of Volatile Methyl

Atmospheric
Chemistry
and Physics
Discussions
Open Access
EGU

591   Siloxanes and their Reaction Products, Chemosphere, 57, 1427-1437,
592   https://doi.org/10.1016/j.chemosphere.2004.08.100, 2004.

593   Wildt, J., Mentel, T., Scharr, A., Hoffmann, T., Andres, S., Ehn, M., Kleist, E., Müsgen, P., Rohrer, F., Rudich, Y.,
594   Springer, M., Tillmann, R., and Wahner, A.: Suppression of New Particle Formation from Monoterpene
595   Oxidation by NO_x, Atmos. Chem. Phys., 14, 2789-2804, https://doi.org/10.5194/acp-14-2789-2014, 2014.

596   Wu, Y. and Johnston, M.: Molecular Characterization of Secondary Aerosol from Oxidation of Cyclic
597   Methylsiloxanes, J. Am. Soc. Mass Spectrom., 27, 402-409, https://doi.org/10.1007/s13361-015-1300-1, 2016.

598   Wu, Y. and Johnston, M.: Aerosol Formation from OH Oxidation of the Volatile Cyclic Methyl Siloxane (cVMS)
599   Decamethylcyclopentasiloxane, Environ. Sci. Technol., 51, 4445-4451,
600   https://doi.org/10.1021/acs.est.7b00655, 2017.

601   Xiao, R., Zammit, I., Wei, Z., Hu, W.-P., MacLeod, M., and Spinney, R.: Kinetics and Mechanism of the Oxidation
602   of Cyclic Methylsiloxanes by Hydroxyl Radical in the Gas Phase: An Experimental and Theoretical Study,
603   Environ. Sci. Technol., 49, 13322-13330, https://doi.org/10.1021/acs.est.5b03744, 2015.

604   Xu, S., Warner, N., Nizzetto, P., Durham, J., and McNett, D.: Long-Range Transport Potential and Atmospheric
605   Persistence of Cyclic Volatile Methylsiloxanes Based on Global Measurements, Chemosphere, 228, 460-468,
606   https://doi.org/10.1016/j.chemosphere.2019.04.130, 2019.

607   Yucuis, R., Stanier, C., and Hornbuckle, K.: Cyclic Siloxanes in Air, Including Identification of High Levels in
608   Chicago and Distinct Diurnal Variation, Chemosphere, 92, 905-910,
609   https://doi.org/10.1016/j.chemosphere.2013.02.051, 2013.

610   Zhao, D., Schmitt, S., Wang, M., Acir, I., Tillmann, R., Tan, Z., Novelli, A., Fuchs, H., Pullinen, I., Wegener, R.,
611   Rohrer, F., Wildt, J., Scharr, A., Wahner, A., and Mentel, T.: Effects of NO_x and SO_2 on the Secondary Organic
612   Aerosol Formation from Photooxidation of α-Pinene and Limonene, Atmos. Chem. Phys., 18, 1611-1628,
613   https://doi.org/10.5194/acp-18-1611-2018, 2018.

614   Zhou, C., Jang, M., and Yu, Z.: Simulation of SOA Formation from the Photooxidation of Monoalkylbenzenes in
615   the Presence of Aqueous Aerosols Containing Electrolytes under Various NO_x Levels, Atmos. Chem. Phys., 19,
616   5719-5735, https://doi.org/10.5194/acp-19-5719-2019, 2019.

617   EUR-Lex: https://eur-lex.europa.eu/legal-
618   content/EN/TXT/?uri=uriserv:OJ.L_.2018.006.01.0045.01.ENG&toc=OJ:L:2018:006:TOCECHA, last
619   access: 25 November 2021, 2018.